The Spine Journal 21 (2021) 1925–1937

Basic Science

The efficacy of a nanosynthetic bone graft substitute as a bone graft extender in rabbit posterolateral fusion

Jordan C. Conway, PhD[a], Rema A. Oliver, PhD[b], Tian Wang, PhD[b], Daniel J. Wills, BVSc[b], Joe Herbert, BVSc[b], Tom Buckland, PhD[a], William R. Walsh, PhD[b], Iain R. Gibson, PhD[a,c,*]

[a] *Sirakoss Ltd., Polwarth Building, Foresterhill, Aberdeen, Scotland, AB25 2ZD, UK*
[b] *Surgical and Orthopedic Research Laboratories, Prince of Wales Clinical School, UNSW Sydney, Level 1, Clinical Sciences Building, Gate 6, Avoca St, Randwick, Sydney, NSW 2031, Australia*
[c] *Institute of Medical Sciences, University of Aberdeen, Foresterhill, Aberdeen, Scotland, AB25 2ZD, UK*
Received 25 February 2021; revised 20 April 2021; accepted 19 May 2021

Abstract

BACKGROUND CONTEXT: Synthetic bone graft substitutes are commonly used in spinal fusion surgery. Preclinical data in a model of spinal fusion to support their efficacy is an important component in clinical adoption to understand how these materials provide a biological and mechanical role in spinal fusion.

PURPOSE: To evaluate the in vivo response of a nanosynthetic silicated calcium phosphate putty (OstP) combined with autograft compared to autograft alone or a collagen-biphasic calcium phosphate putty (MasP) combined with autograft in a rabbit spinal fusion model.

STUDY DESIGN: Efficacy of a nanosynthetic silicated calcium phosphate putty as an extender to autograft was studied in an experimental animal model of posterolateral spinal fusion at 6, 9, 12 and 26 weeks, compared to a predicate device.

METHODS: Skeletally mature female New Zealand White rabbits (70) underwent single level bilateral posterolateral intertransverse process lumbar fusion, using either autograft alone (AG), a nanosynthetic silicated calcium phosphate putty (OstP) combined with autograft (1:1), or a collagen-biphasic calcium phosphate putty (MasP) combined with autograft (1:1). Iliac crest autograft was harvested for each group, and a total of 2 cc of graft material was implanted in the posterolateral gutters per side. Fusion success was assessed at all time points by manual palpation, radiographic assessment, micro-CT and at 12 weeks only using non-destructive range of motion testing. Tissue response, bone formation and graft resorption were assessed by decalcified paraffin histology and by histomorphometry of PMMA embedded sections.

RESULTS: Assessment of fusion by manual palpation at the 12 week endpoint showed 7 out of 8 (87.5%) bilateral fusions in the OstP extender group, 4 out of 8 (50%) fusions in the MasP extender group, and 6 out of 8 (75%) fusions in the autograft alone group. Similar trends were observed with fusion scores of radiographic and micro-CT data. Histology showed a normal healing response in all groups, and increased bone formation in the OstP extender group at all timepoints compared to the MasP extender group. New bone formed directly on the OstP granule surface within the fusion mass while this was not a feature of the Collagen-Biphasic CaP material. After 26 weeks the OstP

FDA device/drug status: Osteo[3] ZP Putty (Approved for this indication), Mastergraft Putty (Approved for this indication).

Author disclosures: ***JCC:*** GRANT: Innovate UK (H, Paid Directly to Institution/Employer). ***RAO:*** Grant: SIRAKOSS (F, Paid Directly to Institution/Employer). ***TW:*** Nothing to disclose. ***DJW:*** Grant: SIRAKOSS (F, Paid Directly to Institution/Employer). ***JH:*** Grant: SIRAKOSS (F, Paid Directly to Institution/Employer). ***TB:*** Nothing to disclose. ***WRW:*** Grant: SIRAKOSS (F, Paid Directly to Institution/Employer). ***IRG:*** Grant: SIRAKOSS Ltd (F, Paid Directly to Institution/Employer) ***JCC:*** Grant: Innovate UK (H, Paid Directly to Institution/Employer); Other (Salary, SIRAKOSS). ***TW:*** Grant: SIRAKOSS (F, Paid Directly to Institution/Employer) ***TB:*** Board of Directors (C, Salary).

Study location: Surgical and Orthopaedic Research Laboratories (SORL), UNSW Sydney, Australia

Ethics: Approved UNSW Animal care and ethics committee 18/115A

*Corresponding author. I.R. Gibson, Institute of Medical Sciences, School of Medicine, Medical Sciences and Nutrition, University of Aberdeen, Foresterhill, Aberdeen, Scotland AB25 2ZD, UK. Tel.: +44-1224-437476; fax: +44-1224-437465.

E-mail address: i.r.gibson@abdn.ac.uk (I.R. Gibson).

https://doi.org/10.1016/j.spinee.2021.05.017

extender group exhibited 100% fusions (5 out of 5) by all measures, whereas the MasP extender group resulted in bilateral fusions in 3 out of 5 (60%), assessed by manual palpation, and fusion of only 20 and 0% by radiograph and micro-CT scoring, respectively. Histology at 26 weeks showed consistent bridging of bone between the transverse processes in the Ost P extender group, but this was not observed in the MasP extender group.

CONCLUSIONS: The nanosynthetic bone graft substituted studied here, used as an extender to autograft, showed a progression to fusion between 6 and 12 weeks that was similar to that observed with autograft alone, and showed excellent fusion outcomes, bone formation and graft resorption at 26 weeks.

CLINICAL SIGNIFICANCE: This preclinical study showed that the novel nanosynthetic silicated CaP putty, when combined with autograft, achieved equivalent fusion outcomes to autograft. The development of synthetic bone grafts that demonstrate efficacy in such models can eliminate the need for excessive autograft harvest and results from this preclinical study supports their effective use in spinal fusion surgery.

Keywords: Posterolateral spinal fusion; Rabbit; Calcium phosphates; Nano-scale morphology; Silicate; Silicon

Introduction

The past two decades has seen a significant number of new synthetic bone grafts products translated from concept to the clinic. Many of these, however, are based on traditional concepts, namely macroporous ceramics of the calcium phosphate phases hydroxyapatite and/or tricalcium phosphate (HA+TCP) [1−5], or bioactive glasses based on sodium-calcium-silicate compositions, particularly 45S5 Bioglass [6−8]. A lack of clinical data on newer products makes comparison with autograft or allograft challenging [9], leading to a lack of clarity of the efficacy of one bone graft substitute over another. The definition of a synthetic bone graft substitute is typically oversimplified, leading to comparisons being made between different products based on a single common feature. There are at least 11 chemical and physical variables that describe fully a synthetic bone graft substitute [10], all of which can have an influence on bone repair.

A number of calcium phosphate-based synthetic bone graft substitutes have been developed in the last decade that build upon the traditional concepts of synthetic bone graft technology. These include the development of chemically modified calcium phosphates [11], incorporation of a submicron surface topography to the granules [1,3] and using nanoscale materials in manufacturing the bone graft [12]. The efficacy of such materials is typically evaluated by comparison to autograft in a pre-clinical model of posterolateral spinal fusion [5,6,13-15], using the validated Boden model in rabbits that shows fusion rates with autograft that are similar to this in humans [16]. A recently published randomised clinical study compared a microporous synthetic bone graft substitute putty, comprising a biphasic composition of HA+TCP, in instrumented posterolateral fusion, compared to autograft [17]. This level 1 study showed non-inferiority of the synthetic material to autograft, based on fusion rates after 12 months from 87 patients.

This study aims to evaluate a novel nanosynthetic silicated calcium phosphate putty in a validated pre-clinical model of posterolateral spinal fusion [5,13,14]. The putty, when combined with equal amounts of autograft, was compared with a commercially available synthetic bone graft substitute putty combined with autograft, and both of these extender groups were compared to the gold standard (autograft alone) after implantation for 6, 9 or 12, which are typical end-points in such studies. Additionally, the two synthetic bone graft groups were compared after implantation for 26 weeks, to provide a longer term evaluation of bone formation and graft resorption.

Materials and methods

Materials

Autograft (AG) bone harvested from the iliac crest was used as the positive control group. Autograft was combined with the materials described below (50/50).

Osteo^3 ZP Putty (SIRAKOSS Ltd., UK) was used as supplied and is referred to as OstP from this point onwards. This material contains 1-2 mm diameter granules of a nanosynthetic silicate-substituted calcium phosphate in a Poloxamer P407 hydrogel carrier.

Mastergraft Putty (Medtronic, Memphis, TN) was used as the predicate. Mastergraft Putty (MasP) is composed of 0.5 mm to 1.6 mm diameter granules of biphasic calcium phosphate (85% B-TCP and 15% hydroxyapatite) dispersed in a bovine type I collagen [18]. MasP has been used successfully as a bone graft extender in rabbit PLF studies [15].

Scanning electron microscopy

Scanning electron microscopy was performed on granules used to prepare the OstP putty samples; granules were deposited onto adhesive carbon on aluminium stubs and coated with a thin layer of Pd/Au. Images were collected using a Carl Zeiss SIGMA VP Analytical Field Emission

Scanning Electron Microscope (Zeiss, Germany). Images were collected using accelerating voltages between 15-20 kV. Average grain sizes were determined by measuring the longest dimension of >100 grains from multiple images at 200,000x magnification using Image J (NIH, USA).

Surgical procedure

The in vivo study was approved by the local Animal Care and Ethics Committee at the (Approval 18/115A) at the UNSW, Australia. A total of 70 adult female New Zealand White rabbits were used in this study, with an allocation summarized in Table 1. Skeletal maturity of each rabbit was verified by radiographic confirmation of growth plate closure at the proximal tibia. The rabbits underwent single-level bilateral posterolateral intertransverse process spine arthrodesis at L4–L5 using established protocols [5,13,14,19].

Surgery followed procedures described elsewhere (add Crowley paper just accepted [5,19]. Briefly, the iliac crest was exposed and corticocancellous bone was harvested and morselised using Rongeur forceps, forming approximately 2cc (~1.6 g) of bone chips ranging from 2 to 5 mm in diameter. For each of OstP and MasP, 1 cc of graft material was combined with 1 cc of autograft to produce an implantable volume of 2 cc per side of the spine; MasP was hydrated, prior to combining with Autograft. For the AG group, 2 cc of autograft was used per side of the spine. Examples of the grafts before and after combination with autograft are shown in Fig. 1(A–D).

Once the rabbit was anesthetised, an incision was made between L3–L5 and the intermuscular plane between the multifidous and longissimus muscles was developed at each level to expose the transverse processes as well as the intertransverse membrane. Host bone between the levels was decorticated using a pneumatic burr. The central region of the transverse processes were decorticated for a distance of 10mm from the vertebral body and pars. At each side of the spine 2 cc of bone graft was placed adjacent to the vertebral body and between the transverse processes, at a distance of 10 mm lateral of the mid-line. Muscle layers were allowed to return to their natural positions and incisions were then closed with 3-0 absorbable sutures. Post-surgery pain was managed with Carprofen (50 mg/ml) at a dose of 4 mg/kg (0.28 mL) SC immediately post-operative on day 1 (24 hours post procedure) and 2 mg/kg (0.14 mL) SC on following days (minimum first 3 days post-operatively). Animals were monitored and observations recorded daily for the first 7 days then weekly thereafter.

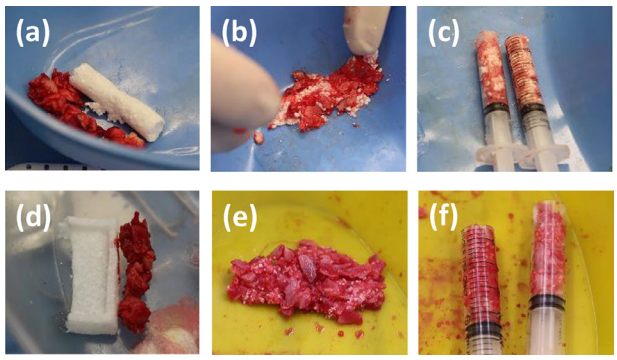

Fig. 1. Preparation of graft volumes for implantation, for OstP (A, B, C) and MasP (D, E, F). Equivalent volumes of the two test articles and iliac crest autograft were measured (A, D), manually combined (B, E), then placed in an open bore syringe to produce 2 cc of graft per syringe (C, F).

Animals were euthanised while under anaesthesia at the study end points; for each study group this was at 6 (n=5), 9 (n=5), 12 (n=8) and 26 (n=5) weeks after surgery (the autograft only group, AG, did not include a 26-week time point as the aim of this later time point was to compare the long term bone formation and graft resorption of the two synthetic bone grafts only). An additional 3 animals were allocated to the two synthetic bone graft test groups to provide a t_0 for histomorphometry, Table 1.

The sample sizes used were based on previous studies using this same model that have been reported in the literatures. For the 12-week time-point the sample size of n=8 per group was chosen to achieve a minimum power of 80% and a level of significance of 5% (two sided) to detect a true difference in the means of the test and predicate group. The observed power for lateral bending was 100% while observed power for flexion extension was 37.9% and 50.4% for flexion-extension and axial rotation, respectively. The sample size at 6, 9 and 26 weeks was n=5 considering range of motion was not performed. The sample sizes were chosen to provide the minimum number of animals to achieve the experimental endpoints and are consistent with similar published studies.

Faxitron radiography

Radiographs of harvested spines were obtained using a Faxitron and digital plates (AGFA CR MD4.0 Cassette). The digital images were processed using an AGFA Digital Developer and workstation (AGFA CR 75.0 Digitiser Musica, AGFA, Germany); the DICOM data were converted to JPEG images using ezDICOM medical viewer.

The radiographic status of the posterolateral spinal arthrodesis for each spine was evaluated from the post-

Table 1
Study end points for the different test groups, showing the number of animals used for each end point

Test Group	0 days	6 weeks	9 weeks	12 weeks	26 weeks
OstP+AG	3	5	5	8	5
MasP+AG	3	5	5	8	5
AG (positive control)	-	5	5	8	-

sacrifice anteroposterior radiographs using the Lenke four-point grading scale [20], as described previously [5,13]. The percentage of successful fusions (grade A) for each level was determined based on image review by two independent observers blinded to both treatment groups and time points.

Micro-CT

Micro computed tomography scanning (53 microns) was performed as previously described [5] all animals following radiography using an Inveon in-vivo micro computed tomography scanner (Siemens Medical, PA, USA) to obtain high resolution radiographic images of the spinal fusions in three planes. Images were examined in the axial, sagittal and coronal planes to assess the overall quality of the fusion mass from transverse process to transverse process as performed for the radiographic data. Fusions at the treated levels were reviewed by two trained and experienced observers in the coronal and sagittal planes in a blinded manner to treatment and time using the four-point Lenke radiographic grading score as described above.

Manual palpation

The stability of the treated levels was assessed by manual palpation [16], blinded by two trained and experienced observers assessed motion in lateral bending and flexion/extension and compared it to the proximal and distal motion segments. The segments were graded as either fused (rigid, no detectable movement at the disc space) or not fused (not rigid, movement detected at the disc space) [5].

Biomechanical testing

Spines were tested non-destructively with pure moments using a Denso robot (simVITRO; Cleveland Clinic BioRobotics Lab, Cleveland, OH) to avoid off axis moments and spurious loading as previously reported [5], in axial rotation (AR), flexion-extension, (FE), and lateral bending (LB). Moments of 270 Nmm were applied [21] at a rate of 33.3 Nmm per second to a maximum of 300 Nmm and was held for 15 seconds. A total of 4.5 load − unload cycles were run in each profile. The last three cycles were analyzed and a mean value at 270 Nmm was taken for each cycle and averaged.

Histology and histomorphometry

The spines were fixed for a minimum of 96 hours in 10% formalin in 0.145 M phosphate buffered saline and cut in the sagittal plane through the middle of vertebral body. One side was randomly processed for decalcified paraffin histology or undecalcified polymethyl methacrylate (PMMA) histology. Paraffin histology was used to assess general tissue response and new bone formation. PMMA histology was used for the quantitative determination of bone formation and graft resorption based on histomorphometry [5].

Specimens were decalcified 10% formic acid in phosphate buffered formalin at room temperature for 3 to 4 days and cut in sagittal plane (~3 mm in thickness), embedded in paraffin and sectioned (5 microns) using a Leica Microtome (Leica Microsystems Pty Ltd, North Ryde, Australia). Sections were stained with H&E and Tetrachrome and examined in a blinded fashion to qualitatively examine local cell and tissue responses using an Olympus light microscope (Olympus, Japan) with a DP72 high-resolution video camera (Olympus, Japan).

PMMA embedded specimens were sectioned in the sagittal plane (~15 micron) using a Leica SP1600 saw-microtome (Leica Microsystems Pty Ltd., North Ryde, Australia) and stained with methylene blue (Sigma, 1% in 0.1 M borax buffer, pH 8.5) and basic fuchsin (Sigma, 0.3% in water) [1]. Three sections were cut from each PMMA block, with a ~2 mm interval to evaluate the entire fusion mass from medial to lateral. Low magnification images were used for histomorphometric analysis [5].

Low magnification images (1.25×, 1 mm scale bar) from the transverse process, the middle of the fusion and the other transverse process were used for quantitative analysis. The region-of-interest was determined by an observer blinded to treatment and time, using a polygon technique [2,5]. The percentage of the graft material or bone tissue (mineralized bone and bone marrow elements) was identified by pixel colour and morphology was determined, and a mean value was obtained, for each animal based.

Statistical analysis

Statistical analysis was performed using GraphPad Prism (v5, GraphPad Software Inc., USA). Grading of spinal fusion (manual palpation, radiographic fusion, and micro-CT fusion) were analysed using a Kruskal-Wallis test with a Dunn's post-test for multiple comparisons. Biomechanical data and histomorphometry data were analysed one-way ANOVA test followed by a Bonferroni post-test for multiple comparisons. Statistically significant differences were considered for values of $p<.05$.

Results

Material characterisation

The morphology of the granules in the OstP was irregular shaped granules with dimensions ranging between 1 mm and 2 mm, Fig. 2(A), and high magnification images show that these have a small sub-micron grain size with a rod-like morphology and have a high level of small sub-micron pores between the grains, Fig. 2(B). The grain size range was between 99 and 237 nm, from a total of 116 grains measured, with a median grain size of 169 nm (standard deviation [SD]=32). The morphology of the granules in MasP have been reported in detail elsewhere [18].

Surgery

No post-surgery complications were observed, and no adverse reactions were observed at any of the end points at the tissue harvest site, gross necropsy of organs, blood analysis or vital organ histology (data not shown). All rabbits were ambulating normally and were clinically normal at each of the end points. Post-operative radiographs confirmed correct placement of the bone grafts.

Radiographic analysis at end-points

Representative radiographs for the three study groups at the end points of 6, 9, 12 and 26 weeks are shown in Fig. 3. The radiographs presented correspond to the third sequentially numbered animal at timepoints with n=5, and the fifth sequentially numbered animal at timepoints with n=8, to attempt a lack of bias in selecting representative images. No migration of the bone grafts from the implantation sites was observed in any of the groups. Radiographs show progression towards a solid fusion mass in the AG, Fig. 3(A, D, G), and OstP groups, Fig. 3(B, E, H, J) with increasing implantation time. For the AG group the individual bone chips that could be observed at 6 weeks could not be easily discriminated at 12 weeks, with mineralised bone bridging the transverse processes. Individual granules were still visible in the OstP group at 12 weeks, and to a lesser extent at 26 weeks, with evidence of trabecular bone within the fusion mass. In the MasP group there was a lack of radiopaque material in the fusion mass by 12 weeks, Fig. 3(I) compared to at 6 and 9 weeks, Fig. 3(C, F), where high contrast calcium phosphate granules in the graft material can be observed. With this loss of contrast of the CaP granules, the morphology of the autologous bone chips can be observed, with significant gaps within the fusion mass.

Examples of 3D micro-CT reconstructions at the 12 week end point for the autograft control, OstP and MasP groups are shown in Fig. 4(A–C), respectively; these correspond to the same animals in Fig. 3(G–I). The graft material in the autograft control group and the OstP group show good integration with the transverse processes, with evidence on new bone throughout the fusion mass, Fig. 4(A and B). Granules can be observed with the graft of the OstP group, but these are integrated within a trabecular network. The MasP group shows limited graft material remaining at the center of the fusion mass, but good integration at the transverse processes, Fig. 4(C). A full panel of micro-CT

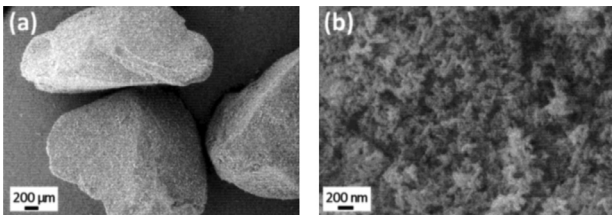

Fig. 2. SEM images (A, B) of the silicated calcium phosphate granule component of OstP.

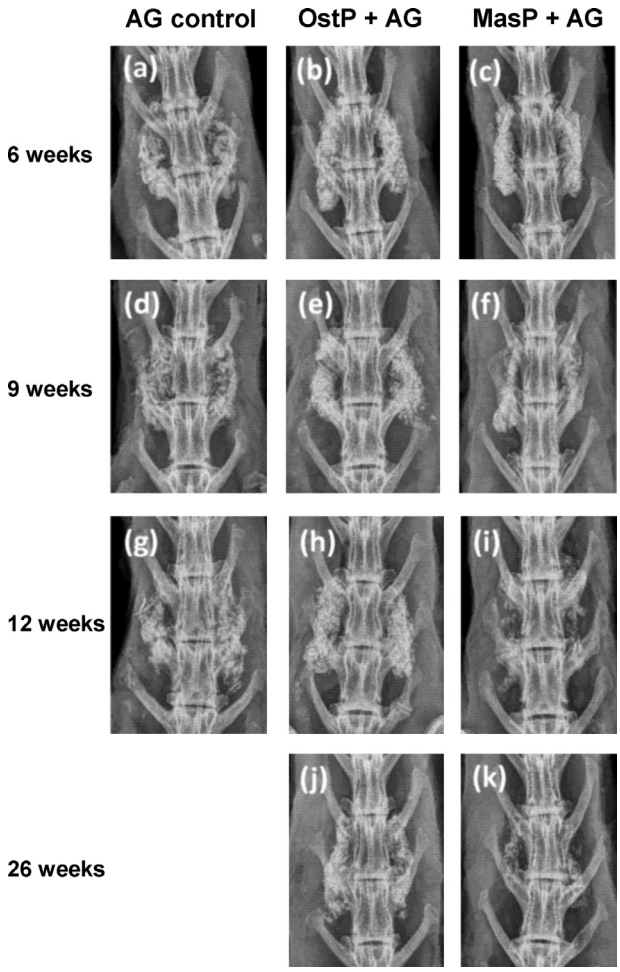

Fig. 3. Representative radiographs for (A, D, G) autograft (AG) control, (B, E, H) OstP+AG, (C, F, I) MasP+AG after the 6, 9 and 12 weeks end-points, respectively. Radiographs for (J) OstP+AG and (K) MasP+AG after the 26 week end-point are included. Images selected correspond to the third sequentially numbered animal for n=5 groups (6, 9 and 26 weeks) and the fifth for n=8 (12 weeks).

reconstructions for all end points are provided in Supplementary Information (Figure S2).

Fusion rate was determined by radiograph grading and micro-CT grading according to the Lenke scale, with fusion rate (%) results corresponding to a Lenke Grade A, solid bilateral fusion, Fig. 5(B and C), respectively. A similar trend is observed with both gradings, although the grading of micro-CT data shows lower scoring at 6 weeks. The autograft (AG) group shows an increase in the fusion rate with increased implantation time up to 12 weeks, reaching 87.5% fusion rate (7 of 8) with both gradings. The OstP group showed an increase in fusion rate with time, reaching 62.5% fusion rate (5 of 8) at 12 weeks and 100% (5 of 5) at 26 weeks, respectively, by both gradings. The MasP group exhibited much lower fusion rates than the other two groups, by both radiograph grading and micro-CT grading. Only 12.5% (1 of 8) spines fused at 12 weeks by micro-CT grading and 0% (0 of 5) after 26 weeks; radiographic grading provided slightly higher rates of 25% (2 of 8) and 20 %

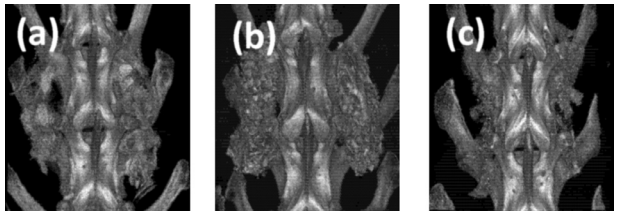

Fig. 4. Representative 3D micro-CT reconstructions at the 12 week endpoint for (A) autograft (AG) control, (B) OstP+AG, (C) MasP+AG. Images selected correspond to the fifth sequentially numbered animal (fifth of eight) for each group.

(1 of 5) at 12 and 26 weeks, respectively. At each of the end points statistically significant differences ($p<.05$) were only observed between the autograft control and the MasP group at 12 weeks, and the OstP and the MasP groups at 26 weeks.

Manual palpation

Bilateral fusion of the spines was also assessed by manual palpation, Fig. 5(A), with fusion rate (%) generally increasing with increased implantation time for each group. Higher fusion rates (%) were observed for the autograft and the OstP groups than the MasP groups at 6 and 9 weeks, and at 12 weeks the manual palpation assessment of bilateral fusion was 75% (6 of 8), 87.5% (7 of 8) and 50% (4 of 8) for the autograft, OstP and MasP groups, respectively. At 26 weeks the fusion rates of the OstP and MasP groups increased further to 100% (5 out of 5) and 60% (3 of 5), respectively. No statistically significant differences were observed between groups at any end point.

Biomechanical assessment

Biomechanical test results of spines at the 12-week endpoint showed that lateral bending range of motion (ROM) showed significant differences between test groups and between the non-operated controls, Fig. 6. The autograft control group and the OstP group showed significantly lower lateral bending ROM ($p<.05$) compared to the non-operated controls, while the mean value for the MasP group was lower but this was not statistically significant; mean values±SD are provided in Table 2. Comparing the OstP and MasP groups showed the lateral bending ROM was significantly lower for the OstP group ($p<.01$). Similar trends were observed for flexion-extension ROM and axial rotation ROM measurements, with the mean values for the three test groups being lower than the non-operated control, but these differences were not statistically significant.

Histological evaluation

Low magnification images of whole spine decalcified histology, with H&E, Fig. 7(A, C, E), or tetrachrome, Fig. 7 (B, D, F) staining for the three study groups at the 12 week end point provide an overview of the healing response;

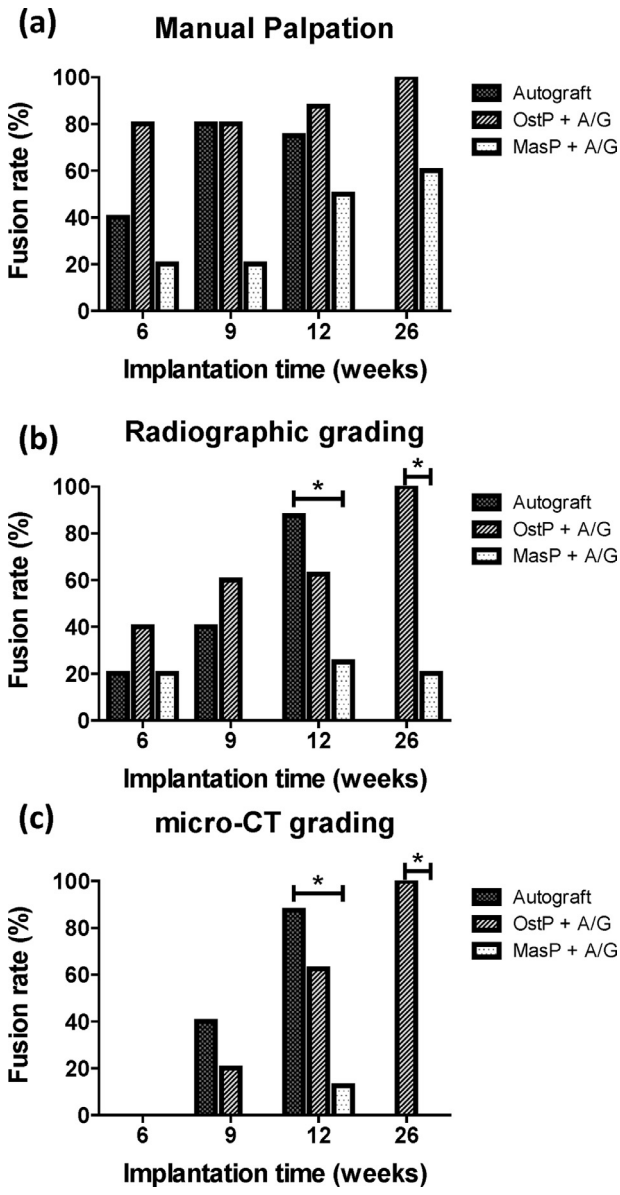

Fig. 5. Assessment of bilateral spinal fusion by (A) manual palpation, (B) radiographic grading and (C) micro-CT grading after 6 (n=5), 9 (n=5), 12 (n=8) or 26 (n=5) weeks (no autograft control at 26 weeks). For radiograph and μCT grading, successful fusion corresponds to a grade A on the Lenke scale. * $p<0.05$.

images are representative sections, with consecutive sections used for the two stains. Transverse processes are highlighted in the tetrachrome stained images and autograft bone and, for OstP and MasP groups, the presence of residual calcium phosphate bone graft is noted. All sections show the presence of bone marrow space in the fusion mass.

Low and high magnification paraffin histology images with tetrachrome staining of areas close to the transverse processes, Fig. 8(A–C), or at the center of the fusion mass, Fig. 8(D–F) for the three groups at 6 weeks are presented. Higher magnification images of the highlighted regions of

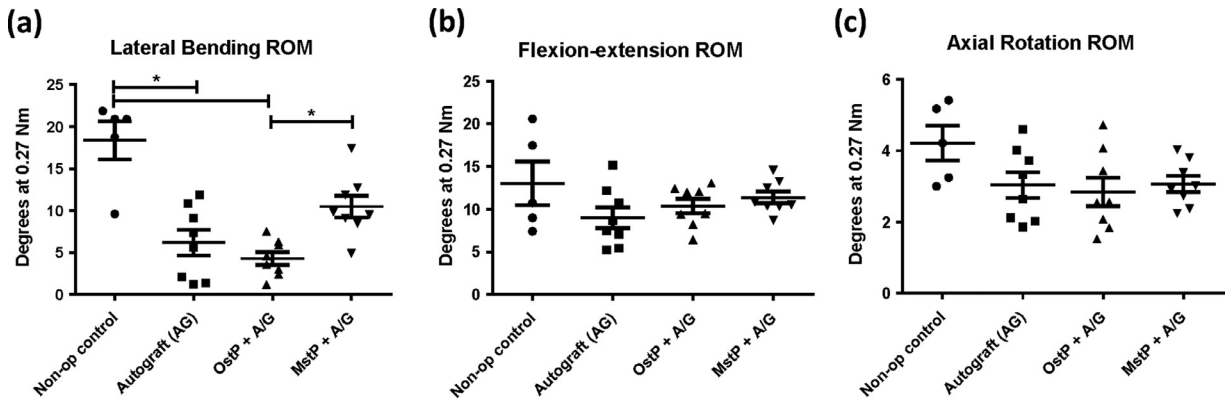

Fig. 6. Biomechanical (ROM) assessment of spinal fusion at 12 weeks. Mean range of motion (˚) by (A) lateral bending, (B) flexion-extension and (C) axial rotation. Data from non-operated controls are included for comparison. Significant differences in lateral bending ROM were found between OstP+AG and MasP+AG groups, and between the non-operated controls and both the AG control and OstP+AG groups, * $p<0.05$ (n=8, except for non-operated controls where n=5)

the images at the center of the fusion mass are presented in Fig. 8(G–I). New bone was observed in the autograft group near the transverse processes and at the center of the fusion mass, Fig. 8(A and D), respectively, with the presence of bone marrow spaces and also chondroblastic tissue which is evidence of regions of bone forming via endochondral ossification (EB). For the OstP group, abundant new bone was observed bridging between granules, and between granules and autograft, near the transverse processes, Fig. 8(B) with bone marrow spaces present. At the center of the fusion mass the maturity of the bone formed between granules was less than at the transverse processes or in the autograft group, but regions of chondroblastic tissue could be observed between granules, indicative of new bone forming via endochondral ossification (EB) by the formation of cartilage-like precursor tissue, Fig. 8(E and H). In the MasP group, new bone could be observed in some regions near the transverse processes but in other areas there was fibrous tissue between the granules, Fig. 8(C). At the center of the fusion mass there was a lack of new bone adjacent to granules with fibrous tissue present between granules and within the macropores, Fig. 8(F and I). No evidence of the Poloxamer gel carrier was observed in histological sections of the OstP group at 6 weeks.

Low and high magnification paraffin histology images with tetrachrome staining of regions at the center of the fusion mass for the OstP, Fig 9(A and C), and MasP, Fig. 9 (B and D), groups at 12 weeks provide a clear comparison of the progression of the healing response at this stage. In the OstP group an outer cortical shell can be observed, with abundant trabecular bone and bone marrow formed in the fusion mass; some granules can still be observed. In the MasP group, an outer cortical shell is not as clear and less bone marrow and new bone is visible, and isolated remnant autograft can be clearly observed. Remnants of the calcium phosphate granules can be observed and these are surrounded in places with a mixed population of inflammatory cells and fibrous tissue, Fig. 9(B and D).

This progression in healing extends to the 26-week time point, with a mature bone repair observed in the fusion mass of the OstP group, with some granules still observed, Fig. 10(A and C). In the MasP group, Fig. 10(B and D), more bone marrow was observed at 26 weeks than at 12 weeks, and more evidence of new bone close to autograft, and individual granules are not clearly identified. The maturity of bone formed in the fusion mass is much less in the MasP group than the OstP group.

Histomorphometric analysis

Histomorphometry was performed on resin-embedded sections (examples of these are shown in supplementary material, Figure S2). An overview of the results is shown in Fig. 11, comparing the amount of new bone formed, consisting of new bone and bone marrow (%bone), residual bone graft remaining (%graft), and soft/fibrous tissue present (%fibrous), at the 6, 9, 12 and 26 week end points. The same data with statistical analysis is included in Figure S3, supplementary material. The autograft (AG) group shows

Table 2
Results of non-destructive biomechanical testing of spine segments after 12 weeks implantation

Test Group	Lateral bending	Flexion-extension	Axial rotation
OstP+AG	4.3±2.2˚ (#, %)	10.4±2.4˚	2.8±1.1
MasP+AG	10.5±3.6˚	11.4±1.9˚	3.1±0.6
AG (positive control)	6.2±4.3˚ (#)	9.0±3.5˚	3.0±1.0
Non-operative control	18.4±5.1˚	13.0±5.7˚	4.2±1.1

Mean range of motion (˚) for lateral bending, flexion-extension and axial rotation of the spine segments in response to pure moment loading (270 Nm). Data presented are Mean±SD. (n=8, except the non-operative controls where n=5). # significantly different from non-operative control ($p<0.05$); % significantly different from MasP+AG ($p<0.01$).

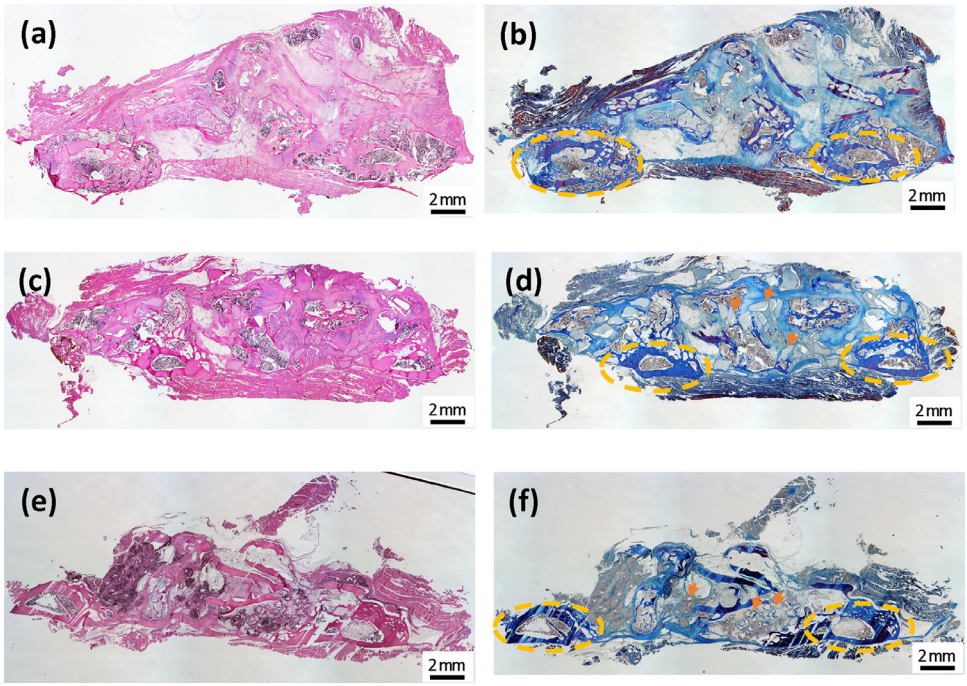

Fig. 7. Low magnification histology images showing the fusion masses of spines 12 weeks after surgery for (A, B) autograft (AG) control group, (c,d) OstP +AG, and (e,f) MasP+AG. Images are stained with H&E (A, C, E) or tetrachrome (B, D, F). Transverse processes are identified in (B), (D) and (F) by orange dashed ovals. Calcium phosphate granules of OstP and MagP can be observed at the center of the fusion mass and near the transverse processes (arrows).

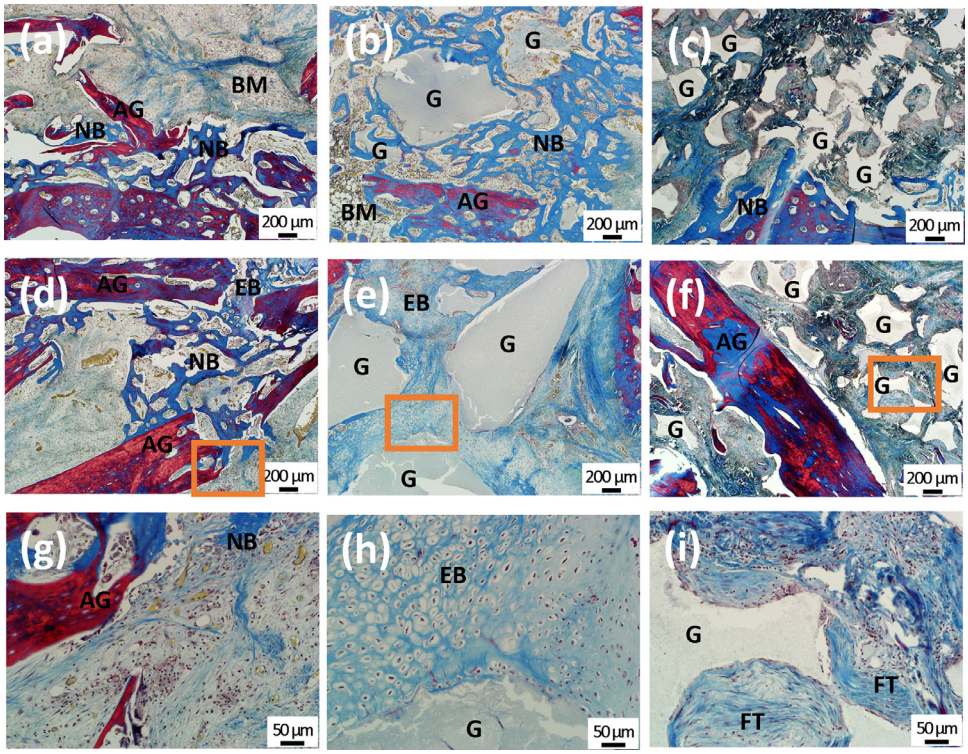

Fig. 8. High magnification paraffin histology images (tetrachrome) of (A, D, G) autograft (AG) control, (B, E, H) OstP+AG and (C, F, I) MasP+AG at 6 weeks after surgery. Representative images close to the transverse processes (A–C) or at the center of the fusion mass (d–f) are presented; higher magnification images of the regions highlighted by the orange boxes in (D–F) are shown in (G–I). G, CaP granules; AG, autograft; FT, fibrous tissue; EB, endochondral bone formation; NB, new bone; BM, bone marrow.

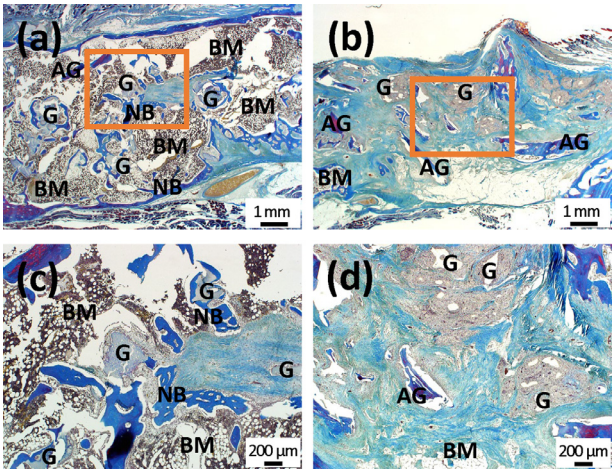

Fig. 9. Low and high magnification paraffin histology images (tetrachrome) of (A, C) OstP+AG and (B, D) MasP+AG at 12 weeks after surgery. Representative images at the center of the fusion mass (A, B) are presented; higher magnification images of the regions highlighted by the orange boxes are shown in (C, D). G, CaP granules; AG, autograft; FT, fibrous tissue; NB, new bone; BM, bone marrow.

the expected increase in new bone and decrease in soft/fibrous tissue with increased implantation time. The OstP group shows a similar progression with time as the autograft group, and also shows a decrease in the residual graft with increased time. The progression in these parameters with time in the MasP group is not so clear. Except for the 9 week time point, there is a trend towards a reduction in residual graft material with increased time. The amount of new bone does not show a clear trend and remains at comparable levels across the time range. The amount of soft/fibrous tissue present from 6 to 12 weeks shows a similar trend to the autograft group, but by 26 weeks the amount of fibrous tissue increases significantly. There was

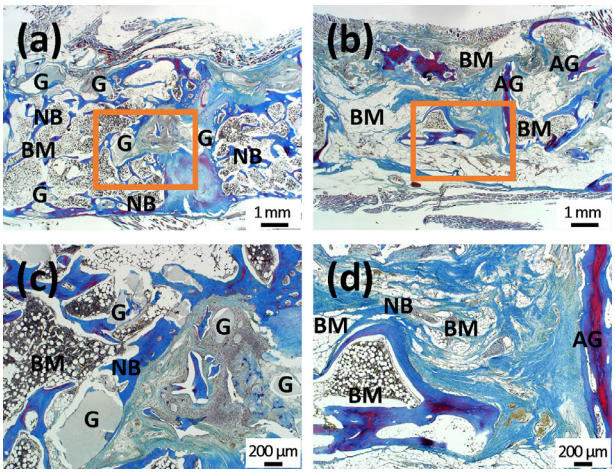

Fig. 10. Low and high magnification paraffin histology images (tetrachrome) of (A, C) OstP+AG and (B, D) MasP+AG at 26 weeks after surgery. Representative images at the center of the fusion mass (A, B) are presented; higher magnification images of the regions highlighted by the orange boxes are shown in (C, D). G, CaP granules; AG, autograft; FT, fibrous tissue; NB, new bone; BM, bone marrow.

significantly more total bone in the OstP group than the MasP group at 9 and 26 weeks, Figure S3(c), and significantly more soft/fibrous tissue in the MasP group than the OstP group at 6 and 26 weeks, Figure S3(d) ($p<.05$). There were no statistically significant differences in the amount of graft material remaining at any of the endpoints between the OstP and MasP groups, Figure S3(e).

Histomorphometry of samples at 26 weeks, Fig. 12(A–J), showed that OstP and MasP behaved similarly when close to the transverse process (TP) (a,c,e,g,i), although the amount of total new bone formed in the OstP group (73.6±8.8%) was significantly greater ($p<.05$) than in the MasP group (64.0±6.9%), with the opposite trend for soft/fibrous tissue (14.8±9.45 vs. 30.4±3.6%, respectively, $p<.05$), Fig. 12 (E and I). A very different response to the two groups was observed at the center of the fusion mass (FM) (b,d,f,h,j), with significantly more total bone in the OstP group than the MasP group (61.0±24.1% vs. 17.4±16.5%, $p<.01$), Fig. 12(F). Comparing the MasP group at the TP and the center of the FM, the raw data for total bone formed and soft/fibrous tissue present at the TP, Fig. 12(E and I) respectively, are very closely distributed around the mean, whereas there is significant scatter in both at the center of the FM, Fig. 12(F and J), and there is significantly less bone and more soft tissue at the center of the FM than at the TP. There were no significant differences in the amount of graft material remaining between the two groups at the TP (15.8±7.2% vs. 17.0±12.4%, $p=.43$) or the center of the FM (11.6±3.1% vs. 7.6±5.8%, $p=.21$), Fig. 12(G and H), suggesting the resorption profiles of the two bone grafts by the 26 week time point were similar.

Discussion

This primary aim of this study was to compare the progression towards fusion of two synthetic bone graft substitutes to the gold standard of autograft in a validated preclinical model of posterolateral fusion between 6 and 12 weeks implantation. The nanosynthetic bone graft substitute studied here (OstP), used as an extender to autograft, exhibited similar end-points to the autograft control, including fusion scores, biomechanical data and general histology.

Although autograft bone harvested from the iliac crest has long been considered the gold standard bone graft, the complications from this additional procedure, most notably donor site pain [22,23], have motivated the search for alternatives. Considerable research has been carried out in the development of improved synthetic calcium phosphate-based bone grafts, which have progressed from the macroporous sintered ceramics of hydroxyapatite (HA), β-tricalcium phosphate (β-TCP) or biphasic calcium phosphate (BCP) that were the basis of many of the clinically used bone graft substitutes of the last 20 years. Examples of these advances include developing synthetic materials that have microstructures that are closer in size-scale to the mineral component of bone [24,25], have a sub-micron

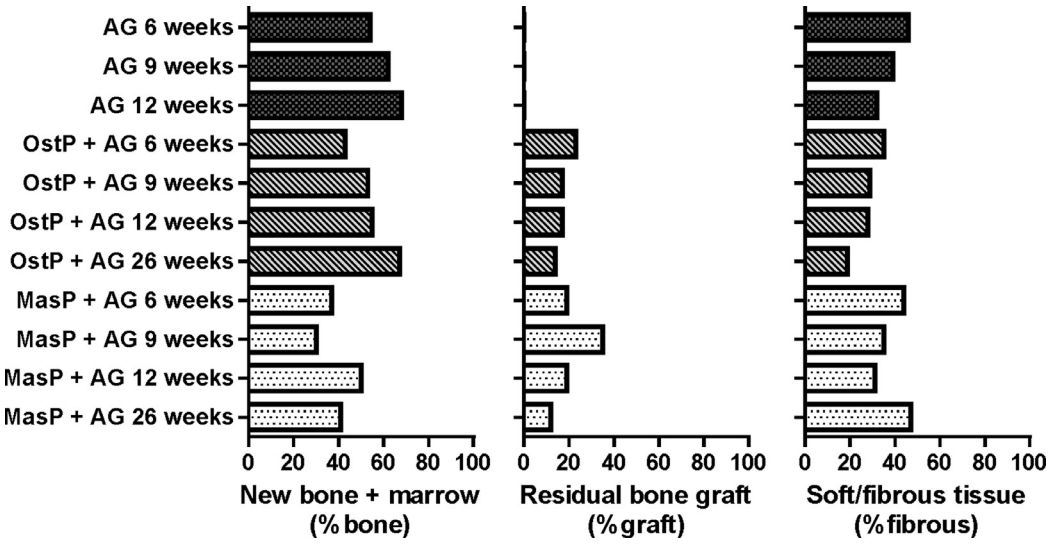

Fig. 11. Overview of histomorphometrical analysis from PMMA-embedded sections showing the data (%) for (A) new bone formed, consisting of new bone +bone marrow (%bone), (B) residual bone graft material remaining (%graft) and (C) soft/fibrous tissue (%fibrous) in the fusion mass over time, at 6, 9, 12 and 26 weeks (n=8 at 12 weeks, n=5 at all other time points, data represent mean values). Autograft control (AG) not included at 26 weeks. Full data sets including mean, SEM and statistical analysis available in Figure S2 (supplementary information).

topography [3,5] or introduce larger quantities of microporosity [11], with these having the effect of increasing the surface area of the material. For example, decreasing the grain size of β -TCP granules from 2.50 to 0.81 μm, corresponding with an increase in the surface area from 0.7 to 1.4 m^2/g, significantly increased the amount of bone formed and the amount of material resorbed when implanted both intramuscularly and in posterolateral fusion in canines after 12 weeks [26]. Similarly, decreasing the median grain size of BCP granules from 1.52 to 0.6 μm, which was associated with an increase in surface area from 1.21 to 2.77 m^2/g, significantly increased the amount of bone formed and the amount of graft material resorbed when implanted intramuscularly in canines up to 12 weeks [3]. The performance of these BCP granules, including as a putty of the granules dispersed in a resorbable polymeric carrier, as an extender to autograft in the rabbit PLF model showed equivalent fusion rates to an autograft control [5].

In the present study a novel nanosynthetic bone graft substitute was evaluated as an extender to autograft in a recognised preclinical model for spinal fusion. The material, Osteo^3 ZP Putty (OstP), consisted of granules of silicated calcium phosphate in an aqueous poloxamer carrier. The granules are described as containing approximately 5.8 weight % silicon substituted into the calcium phosphate phase, and have a porosity >75%; the putty contains 30% granules and 70% poloxamer gel, by weight. These granules consist of very small grains (<250 nm) and micropores (<1 μm), Fig. 2(B). The OstP material was compared with another putty-like synthetic bone graft substitute, MasP, which has been characterized extensively elsewhere; briefly it is a mixture of granules of a biphasic β-TCP and HA at a ratio of 85:15%, combined with bovine type I collagen which forms a putty when mixed with water or saline [18].

In this study, the synthetic bone grafts were each combined with autograft to produce a volume of 4 cc of a 1:1 mixture per animal, with a graft volume of 2 cc per side of the spine. The effect of graft volume of autograft in the rabbit PLF model has been reported to negatively affect fusion rates when small volumes (≤1 cc per side) are used, but no significant difference in fusion rate observed for graft volumes > 1 cc up to 3 cc per side [27]. This is therefore important when using the rabbit PLF model for studying synthetic bone grafts as extenders to autograft, as it could be possible that for a total graft volume of 3 cc per side, the graft would contain sufficient autograft (1.5 cc) to lead to a successful fusion, irrespective of the efficacy of the synthetic bone graft. Using a graft volume of 2 cc per side in the extender groups means that there is insufficient autograft present to lead to typical fusion rates for autograft, therefore providing a true test of the synthetic graft extender [28]. Implantations were performed at the L4–L5 vertebral level which has been shown to have no significant effect on fusion rate compared to the L5-–L6 level [27,29].

The fusion rate for the positive control group were consistent with reported studies [5,13,19,30]. Biomechanical analysis of spines at 12 weeks showed a decrease in all range of motions compared to non-operative controls in the autograft group, with the decrease in lateral bending ROM being statistically significant. Progression towards increased fusion and bone formation throughout the fusion mass were observed in the autograft group from grading of the fusions by manual palpation, radiographs, and micro-CT, and from histology and histomorphometry. Observations were consistent with previous studies in our labs and with published studies, confirming that the autograft group served as an appropriate positive control arm in this study.

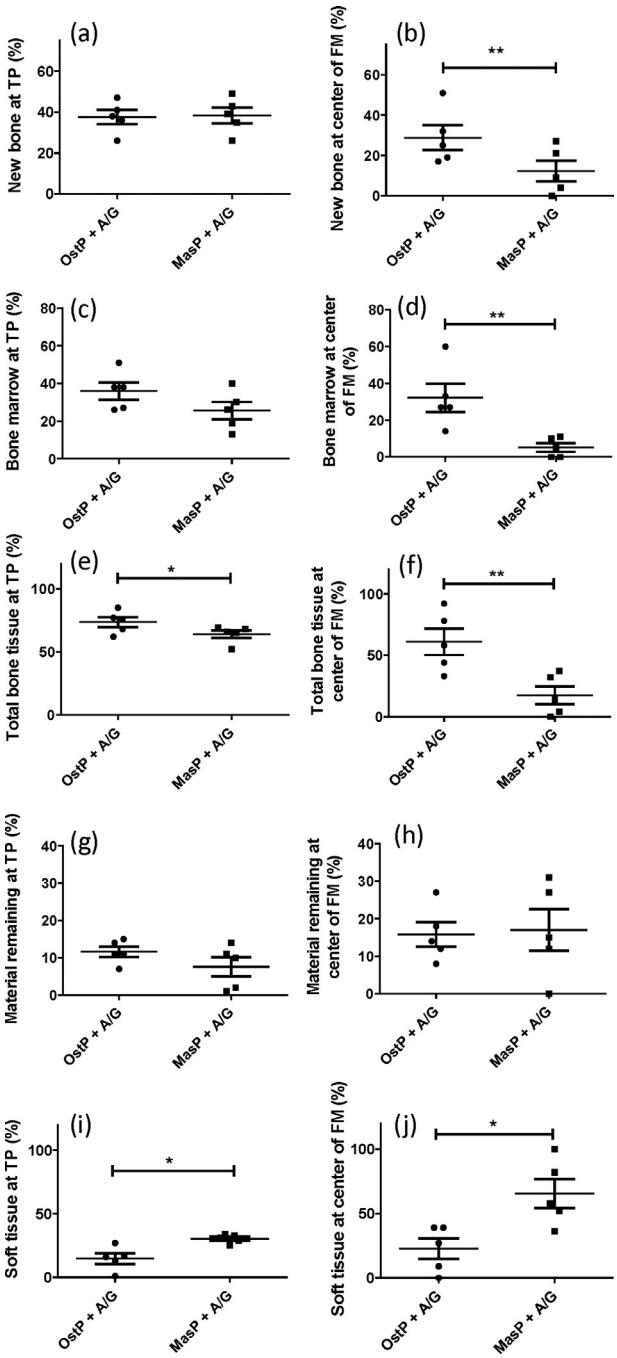

Fig. 12. Detailed histomorphometrical analysis at 26 weeks from PMMA-embedded sections comparing data from regions near the transverse processes (TP) (A, C, E, G, I) and at the center of the fusion mass (FM) (B, D, F, H, J) for the two synthetic bone grafts materials, OstP and MasP, combined with autograft. The data (%) are for (A and B) new bone formed, (C and D) bone marrow formed, (E and F) total new bone (new bone+bone marrow), (G and H) graft material remaining, (I and J) soft tissue. Individual data points are shown, with horizontal bars showing mean values and st. dev. (n=5). * p<.05.

The synthetic bone graft comparator group, MasP, did not perform as well as the autograft group, with significantly lower fusion rates at 12 weeks by grading of radiographs and micro-CT, Fig. 5, and less total bone formed at 6, 9 or 12 weeks, Fig. 11 and S3. Fusion rate by manual palpation for the MasP group, and progression to bone repair and graft resorption from histology, were observed with increasing implantation time, but in this study MasP as an extender to autograft was not equivalent to autograft. A number of studies have reported the use of MasP, or a comparable form Mastergraft Strip, in the rabbit PLF model and have reported varying responses. When MasP was combined with autograft (50%) and implanted at volumes of 3 cc per side, fusion rates by manual palpation and radiographic scoring after 8 weeks were 73% and 91%, respectively [15], which are significantly greater than any fusion rate in the present study. When Mastergraft Strip was combined with autograft (50%), again implanting 3 cc of graft per side, a fusion rate of 75% was determined by manual palpation and radiographic scoring after 8 weeks [31]. In contrast, a study of similar design reported a fusion rate by manual palpation of only 12.5% after 8 weeks for Mastergraft Strip combined with autograft (50%) [32]. In the present study a fusion rate of 20% (1/5) at the 9 week time-point was determined by manual palpation in the MasP group, but 0% (0/5) by grading of radiographs or micro-CT reconstructions. Fusion rates by manual palpation increased to 40 and 60% at 12 and 26 weeks, but these values were higher than fusion rates by grading of radiographs or micro-CT reconstructions. This is consistent with the lack of bridging mineralised tissue/graft in the radiographs and micro-CT, Fig. 3(I and K) and Fig. 4(C), and lack of new bridging bone through the fusion mass by histology. The differences may be a result of different graft volumes used, or differences in combination of the putty and the autograft. Separation of the histomorphometry results at the 26 week end-point into regions close to the transverse processes (TP) and the center of the fusion mass (FM) showed that the MasP group performed significantly better close to the TP than the center of the FM, with more bone formed, less graft remaining and less soft/fibrous tissue remaining close to the TP than at the center of the FM, Fig. 12(C, D, E). It is feasible that a longer time-point may lead to progressive osteoconduction from the bone formed close to the TPs throughout the fusion mass and lead to bridging fusions.

The OstP group showed a comparable behaviour to the autograft control group. No statistically significant differences were observed in the fusion rates between these two groups at any endpoint by the three methods of grading, and no significant differences in any of the measured ROMs at the 12-week end-point. Excluding the presence of graft material in the OstP group, the two groups showed a similar trend in increasing total bone and decreasing soft/fibrous tissue with increasing implantation time from 6 to 12 weeks. Regions of chondroblastic tissue in the center of the fusion mass were observed in the histology of the OstP group and the autograft group at 6 weeks, which is indicative of endochondral bone formation. This may lead to the progression towards bridging bone through the fusion mass and to the higher fusion rates observed with these two

groups, compared to the MasP group. The data for the 6, 9 and 12-week end-points supports that OstP is an effective extender to autograft, providing an alternative to harvesting large volumes of autograft bone.

The OstP group achieved 100% fusion (5 out of 5) by manual palpation, radiographic grading and micro-CT grading at the 26-week endpoint, and for the last two gradings this fusion rate was statistically greater than the MasP group. Histomorphometry results of regions close to the TP and at the center of the FM showed similar results for total bone formed and graft material remaining for the OstP group, suggesting that at 26 weeks the progression of bone formation and fusion were consistent throughout the fusion mass, as opposed to the bimodal response at the TP and FM observed in the MasP group at 26 weeks, Fig. 12. Comparison of the graft material remaining after 26 weeks showed a similar amount of material for the two synthetic materials. MasP is a biphasic calcium phosphate (BCP) composed of predominantly β-TCP (85%) and these compositions have been shown to exhibit enhanced resorption *in vivo* compared to hydroxyapatite (HA)-based ceramic synthetic materials; the OstP material therefore shows an *in vivo* resorption profile that is closer to BCP than HA.

There are some of limitations of this study, most importantly being that, although this preclinical model exhibits a comparable level of fusion success for autograft to human, it may not predict human clinical performance of bone grafts. The study did not include autograft at the 26-week endpoint as the aim of this additional time point was to compare the two synthetic materials; the inclusion of this would have provided some more context to the observation of the OstP group achieving 100% fusion (5/5) by all measures at this time-point. It would be interesting to test different graft volumes, but also different amounts of autograft used as extender (25 and 75%), but this was beyond the scope of this study. Similarly, the inclusion of earlier (3 weeks), intermediate (18 weeks) and long-term (52 weeks) end-points could provide a more complete assessment of progression of healing, fusion, remodelling and graft resorption. Immunohistochemistry could provide some extra insights, in particular if there is evidence of graft influence on the early inflammatory response, in particular macrophage polarisation, the role of osteoclast activity in the remodelling of the two graft materials, and possibly the tissue source of mesenchymal stem cells that led to the formation of chondroblastic tissue at the center of the fusion mass in the autograft and OstP groups at 6 weeks, Fig. 8(D and E). The rabbit PLF model has been used extensively to evaluate various bone graft materials, but it is an uninstrumented model and the biomechanics of the rabbit spine are different to humans. Evaluation of these materials in an instrumented model of posterolateral spinal fusion would provide further insight to their performance compared to autograft, but the data from this study shows that in a demanding preclinical model the OstP Putty may be used effectively as a bone graft extender.

The OstP material studied here contains silicated calcium phosphate granules with much higher levels of silicon/silicate substituted in the apatite structure than other silicated calcium phosphate bone grafts that have been used clinically [33,34], but also a much smaller grain size. These properties have not been correlated with *in vivo* bone formation in this system, but studies on other systems such as tricalcium phosphate (β-TCP) and biphasic calcium phosphate (BCP) materials have shown that bone formation can be positively affected by relatively small decreases in grain size [3,5,26].

In conclusion, the novel nanosynthetic silicate calcium phosphate (OstP) studied as a bone graft extender in an established preclinical model of posterolateral fusion exhibited similar performance to autograft alone, with no statistically significant differences observed between these groups in fusion grading (manual palpation, radiographs or μCT) or biomechanical testing at 12 weeks (n=8). The inclusion of a 26 week time point in this study to compare the two synthetic bone graft substitutes showed that bone formation and graft resorption for the OstP material continued beyond the typical 12 week end point and led to fusion in all animals by all assessment methods. These findings conclude that this material demonstrates excellent efficacy as an extender to autograft in the Boden preclinical model of posterolateral fusion.

Acknowledgments

This study was partly funded by a grant from Innovate UK (Grant no. 103853), awarded to Sirakoss Ltd., with the remaining study costs provided by Sirakoss Ltd.

Declarations of Competing Interests

The authors declare that they have no known competing financial interests or personal relationships that could have appeared to influence the work reported in this paper.

Supplementary materials

Supplementary material associated with this article can be found in the online version at https://doi.org/10.1016/j.spinee.2021.05.017.

References

[1] Yuan H, Fernandes H, Habibovic P, de Boer J, Barradas AMC, de Ruiter A, et al. Osteoinductive ceramics as a synthetic alternative to autologous bone grafting. Proc Natl Acad Sci USA 2010;107:13614–9. https://doi.org/10.1073/pnas.1003600107.

[2] Walsh WR, Oliver RA, Christou C, Lovric V, Walsh ER, Prado GR, et al. Critical size bone defect healing using collagen-calcium phosphate bone graft materials. PLoS One 2017 Jan 3;12:e0168883. https://doi.org/10.1371/journal.pone.0168883.

[3] Duan R, van Dijk LA, Barbieri D, de Groot F, Yuan H, de Bruijn JD. Accelerated bone formation by biphasic calcium phosphate with a novel sub-micron surface topography. Eur Cell Mater 2019;37:60–73. https://doi.org/10.22203/eCM.v037a05.

[4] Pereira RC, Benelli R, Canciani B, Scaranari M, Daculsi G, Cancedda R, et al. Beta-tricalcium phosphate ceramic triggers fast and robust bone formation by human mesenchymal stem cells. J Tissue Eng Regen Med 2019;13:1007–18. https://doi.org/10.1002/term.2848.

[5] van Dijk LA, Barbieri D, Barrère-de Groot F, Yuan H, Oliver R, Christou C, et al. Efficacy of a synthetic calcium phosphate with submicron surface topography as autograft extender in lapine posterolateral spinal fusion. J Biomed Mater Res Part B Appl Biomater. 2019;107B:2080–90. https://doi.org/10.1002/jbm.b.34301.

[6] Fredericks D, Petersen EB, Watson N, Grosland N, Gibson-Corley K, Smucker J. Comparison of two synthetic bone graft products in a rabbit posterolateral fusion model. Iowa Orthop J 2016;36:167–73.

[7] Pugely AJ, Petersen EB, DeVries-Watson N, Fredericks DC. Influence of 45S5 bioactive glass in a standard calcium phosphate collagen bone graft substitute on the posterolateral fusion of rabbit spine. Iowa Orthop J 2017;37:193–8.

[8] Westhauser F, Karadjian M, Essers C, Senger A-S, Hagmann S, Schmidmaier G, et al. Osteogenic differentiation of mesenchymal stem cells is enhanced in a 45S5-supplemented β-TCP composite scaffold: an in-vitro comparison of Vitoss and Vitoss BA. PLoS One 2019;14:e0212799. https://doi.org/10.1371/journal.pone.0212799.

[9] Buser Z, et al. Synthetic bone graft versus autograft or allograft for spinal fusion: a systematic review. J Neurosurg Spine 2016;25:509–16. https://doi.org/10.3171/2016.1.SPINE151005.

[10] Published by Editor Gibson IR. Chapter 12 - Synthetic hydroxyapatite for bone-healing applications. In: Mucalo M, editor. Published by Editor, 2015, editor. Hydroxyapatite (HAp) for Biomedical Applications. 1st Edition Woodhead Publishing; 2015. Published by Editor.

[11] De Godoy RF, Hutchens S, Campion C, Blunn G. Silicate-substituted calcium phosphate with enhanced strut porosity stimulates osteogenic differentiation of human mesenchymal stem cells. J Mater Sci Mater Med 2015;26:54. https://doi.org/10.1007/s10856-015-5387-5.

[12] Dau M, Ganz C, Zaage F, Staedt H, Goetze E, Gerber T, et al. In vivo comparison of a granular and putty form of a sintered and a non-sintered silica-enhanced hydroxyapatite bone substitute material. J. Biomater. Appl. 2020;34:864–74. https://doi.org/10.1177/0885328219877584.

[13] Walsh WR, Vizesi F, Cornwall GB, Bell D, Oliver RA, Yu Y. Posterolateral spinal fusion in a rabbit model using a collagen-mineral composite bone graft substitute. Eur Spine J 2009;18:1610–20. https://doi.org/10.1007/s00586-009-1034-5.

[14] Walsh WR, Oliver RA, Gage G, Yu Y, Bellemore J, Adkisson HD. Application of resorbable poly(lactide-co-glycolide) with entangled hyaluronic acid as an autograft extender for posterolateral inter-transverse lumbar fusion in rabbits. Tissue Eng A 2011;17:213–20. https://doi.org/10.1089/ten.TEA.2010.0008.

[15] Smucker JD, Petersen EB, Fredericks DC. Assessment of MASTERGRAFT PUTTY as a graft extender in a rabbit posterolateral fusion model. Spine (Phila Pa 1976) 2012;37:1017–21. https://doi.org/10.1097/BRS.0b013e31824444c4.

[16] Boden SD, Schimandle JH, Hutton WC. An experimental lumbar intertransverse process spinal fusion model: Radiographic, histologic, and biomechanical healing characteristics. Spine 1995;20:412–20. https://doi.org/10.1097/00007632-199502001-00003.

[17] Lehr AM, Oner FC, Delawi D, Stellato RK, Hoebink EA, Kempen DHR, et al. Efficacy of a standalone microporous ceramic versus autograft in instrumented posterolateral spinal fusion: a multicenter, randomized, intrapatient controlled, noninferiority trial. Spine (Phila Pa 1976) 2020;45:944–51. https://doi.org/10.1097/BRS.0000000000003440.

[18] Bumgardner JD, Wells CM, Haggard WO. Ceramic composites for bone graft applications from: translating biomaterials for bone graft, bench-top to clinical applications. CRC Press; 2016.

[19] Crowley JD, Oliver RA, Dan MJ, Wills DJ, Rawlinson JW, Crasto RA, et al. Single level posterolateral lumbar fusion in a New Zealand White rabbit (Oryctolagus cuniculus) model: Surgical anatomy, operative technique, autograft fusion rates, and perioperative care. JOR Spine 2020:e1135. https://doi.org/10.1002/jsp2.1135.

[20] Lenke LG, Bridwell KH, Bullis D, Betz RR, Baldus C, Schoenecker PL. Results of in situ fusion for isthmic spondylolisthesis. J Spinal Disord 1992;5:433–42. https://doi.org/10.1097/00002517-199212000-00008.

[21] Grauer JN, Erulkar JS, Patel TC, Panjabi MM. Biomechanical evaluation of the New Zealand white rabbit lumbar spine: a physiologic characterization. Eur Spine J 2000;9:250–5. https://doi.org/10.1007/s005860000141.

[22] Summers BN, Eisenstein SM. Donor site pain from the ilium. A complication of lumbar spine fusion. J Bone Joint Surg Br 1989;71:677–80. https://doi.org/10.1302/0301-620X.71B4.2768321.

[23] Fernyhough JC, Schimandle JJ, Weigel MC, Edwards CC, Levine AM. Chronic donor site pain complicating bone graft harvesting from the posterior iliac crest for spinal fusion. Spine (Phila Pa 1976) 1992;17:1474–80. https://doi.org/10.1097/00007632-199212000-00006.

[24] Harms C, Helms K, Taschner T, Stratos I, Ignatius A, Gerber T, Lenz S, et al. Osteogenic capacity of nanocrystalline bone cement in a weight-bearing defect at the ovine tibial metaphysis. Int J Nanomedicine 2012;7:2883–9. https://doi.org/10.2147/IJN.S29314.

[25] Duan R, Barbieri D, Luo X, Weng J, Bao C, de Bruijn JD, et al. Variation of the bone forming ability with the physicochemical properties of calcium phosphate bone substitutes. Biomater Sci 2017;6:136–45. https://doi.org/10.1039/c7bm00717e.

[26] Duan R, Barbieri D, Luo X, Weng J, de Bruijn JD, Yuan H. Submicron-surface structured tricalcium phosphate ceramic enhances the bone regeneration in canine spine environment. J Orthop Res 2016;34:1865–73. https://doi.org/10.1002/jor.23201.

[27] Riordan AM, Rangarajan R, Balts JW, Hsu WK, Anderson PA. Reliability of the rabbit postero-lateral spinal fusion model: A meta-analysis. J Orthop Res 2013;31:1261–9. https://doi.org/10.1002/jor.22359.

[28] Curylo LJ, Johnstone B, Petersilge CA, Janicki JA, Yoo JU. Augmentation of spinal arthrodesis with autologous bone marrow in a rabbit posterolateral spine fusion model. Spine 1999;24:434–8. https://doi.org/10.1097/00007632-199903010-00004.

[29] Ghodasra JH, Daley EL, Hsu EL, Hsu WK. Factors influencing arthrodesis rates in a rabbit posterolateral spine model with iliac crest autograft. Eur Spine J 2014;23:426–34. https://doi.org/10.1007/s00586-013-3074-0.

[30] Kiely PD, Brecevich AT, Taher F, Nguyen JT, Cammisa FP, Abjornson C. Evaluation of a new formulation of demineralized bone matrix putty in a rabbit posterolateral spinal fusion model. Spine J 2014;14:2155–63. https://doi.org/10.1016/j.spinee.2014.01.053.

[31] Smucker JD, Petersen EB, Nepola JV, Fredericks DC. Assessment of Mastergraft(®) strip with bone marrow aspirate as a graft extender in a rabbit posterolateral fusion model. Iowa Orthop J 2012;32:61–8.

[32] Miller CP, Jegede K, Essig D, et al. The efficacies of 2 ceramic bone graft extenders for promoting spinal fusion in a rabbit bone paucity model. Spine (Phila Pa 1976) 2012;37:642–7. https://doi.org/10.1097/BRS.0b013e31822e604e.

[33] Coughlan M, Davies M, Mostert AK, et al. A prospective, randomized, multicenter study comparing silicated calcium phosphate versus BMP-2 synthetic bone graft in posterolateral instrumented lumbar fusion for degenerative spinal disorders. Spine (Phila Pa 1976) 2018;43:E860–8. https://doi.org/10.1097/BRS.0000000000002678.

[34] Bolger C, Jones D, Czop S. Evaluation of an increased strut porosity silicate-substituted calcium phosphate, SiCaP EP, as a synthetic bone graft substitute in spinal fusion surgery: a prospective, open-label study. Eur Spine J 2019;28:1733–42. https://doi.org/10.1007/s00586-019-05926-1.